11296 *Biochemistry* **2009,** *48,* 11296–11303
DOI: 10.1021/bi9017297

BIOCHEMISTRY
including biophysical chemistry & molecular biology
Article

Mechanism of the Translation Termination Reaction on the Ribosome[†]

Stefan Trobro and Johan Åqvist*

Department of Cell and Molecular Biology, Uppsala University, Biomedical Center, Box 596, SE-751 24 Uppsala, Sweden

Received October 7, 2009; Revised Manuscript Received November 2, 2009

ABSTRACT: Ribosomal release factors (RFs) catalyze the termination of protein synthesis by triggering hydrolysis of the peptidyl−tRNA ester bond in the peptidyl transferase center of the ribosome. With new medium-resolution crystallographic structures of RF−ribosome complexes available, it has become possible to examine the detailed mechanism of this process to resolve the key factors responsible for catalysis of the termination reaction. Here, we report computer simulations of the termination reaction that utilize both the new RF complex structures and information from a high-resolution complex with a P-site substrate analogue. The calculations yield a consistent reaction mechanism that reproduces experimental rates and allows us to identify key interactions responsible for the catalytic efficiency. The results are also in general agreement with an earlier model based on molecular docking. The methylated glutamine residue of the universally conserved GGQ motif plays a key role in the hydrolysis reaction by orienting the water nucleophile and by stabilizing the transition state, and its side chain makes an entropic contribution to the lowering of the activation barrier. Two additional water molecules interacting with the P-site substrate are also found to be critically important. Furthermore, the 2′-OH group of the peptidyl−tRNA substrate is predicted to act as a proton shuttle for the leaving group in analogy with the consensus mechanism for peptidyl transfer. Thus, the ribosome's ability to catalyze both the termination (hydrolysis) and peptidyl transfer (aminolysis) reactions is largely explained by this type of unified mechanism, with similar transition states occurring in both processes.

The protein synthesis machinery utilizes different types of translation factors for initiation, elongation, and termination. Class 1 release factors (RFs)[1] catalyze the hydrolysis of the ester bond between the nascent peptide chain and the tRNA in the ribosomal P-site, thus releasing the newly synthesized polypeptide from the ribosome. This occurs when a stop codon is exposed by the mRNA in the ribosomal A-site, and, in bacteria, RF1 recognizes the UAA and UAG stop codons while RF2 reads the UAA and UGA codons. Binding of RF1 or RF2 to the decoding center on the small ribosomal subunit positions the universally conserved GGQ motif in domain 3 of the RFs in such a way as to promote hydrolysis of the peptidyl−tRNA bond in the peptidyl transferase center (PTC) on the large subunit (~75 Å from the decoding center). Although the RFs were discovered already more than four decades ago (*1*), it is only relatively recently that their detailed mechanism of action has begun to be understood. Nakamura and co-workers (*2*) showed the importance of specific tripeptide motifs, P(A/V)T in RF1 and SPF in RF2, in determining stop codon specificity, while the universally conserved GGQ tripeptide sequence was shown to be essential for promoting the hydrolysis reaction leading to peptide release (*3*). Moreover, the conserved Gln residue in the latter motif is N5-methylated (*4*), and this methylation has a significant effect on both termination rates and bacterial growth (*4*, *5*).

On the structural side, the first three-dimensional information about interactions between RFs and ribosomes was provided by low-resolution (~6 Å) crystal structures of 70S *Thermus thermophilus* complexes with RF1 and RF2 (*6*) and by 11−14 Å resolution cryo-electron microscopy models (*7*, *8*). These studies showed that the conformations of RF1 and RF2 bound to the ribosome are similar to their solution structures (*9*) but differ from the corresponding crystal structures of free release factors (*10*, *11*). While the low-resolution X-ray structures (*6*) showed approximately where the PVT/SPF and GGQ loops were located in the ribosome complexes, no detailed information regarding atomic interactions could be attained at this resolution.

To investigate the role of the characteristic GGQ motif in promoting cleavage of the peptidyl−tRNA bond, we conducted molecular docking calculations (*12*) for the ribosome with a heptapeptide containing GGQ (with sequence PGGQ^{me}GVN derived from the *T. thermophilus* RFs). These calculations were done with a fully flexible peptide and a rigid ribosome structure, but the ends of the peptide backbone were softly constrained to their observed positions in the low-resolution crystal structures (*6*). The solutions from these docking calculations were then subjected to molecular dynamics (MD) simulations of free energy profiles for the peptidyl−tRNA hydrolysis reaction, utilizing the empirical valence bond (EVB) method in combination with the free energy perturbation (FEP) technique (*13*, *14*). The strategy was thus to explore what conformations of the GGQ loop could give rise to catalysis of the termination reaction.

The results from these simulations showed a unique type of conformational solution with the ability to catalyze the reaction, where the Gln side chain inserts deeply into the A-site and coordinates a hydrolytic water molecule with its carbonyl group (*12*). This model reproduced observed reaction rates, including the effects of several mutations, and predicted the viability of a proton shuttle mechanism akin to that of the

[†]Support from the Swedish Research Council (VR) is gratefully acknowledged.

*To whom correspondence should be addressed. Phone: +46 18 471 41 09. Fax: +46 18 53 69 71. E-mail: aqvist@xray.bmc.uu.se.

[1]Abbreviations: RF, release factor; PTC, peptidyl transferase center; MD, molecular dynamics; EVB, empirical valence bond; FEP, free energy perturbation; PDB, Protein Data Bank.

 Published on Web 11/02/2009

peptidyl transfer reaction (*15*−*18*). It should be noted here that insertion of the Gln residue into the A-site in such a way that it makes contact with the P-site substrate was far from obvious from the existing experimental data. In fact, several other somewhat vaguer conceptual models rather invoked indirect effects of the GGQ loop in promoting catalysis (*19*−*22*). However, recent experiments from Green and co-workers (*23*, *24*) have provided further support for the model of Trobro and Åqvist (*12*). First, it was shown that the specificity of the RF for water as a nucleophile in the termination reaction depended critically on the length of the side chain at the Gln position (*23*). The experiments showed that with the native Gln residue only water could act as a nucleophile, but that with smaller side chains larger nucleophiles (hydroxylamine, methanol, and ethanol) became reactive. Second, it was found, just as for the peptidyl transfer reaction (*16*), that A76 2′-deoxy or fluoro-substituted P-site substrates were inactive in the termination reaction (*24*), supporting a key role of the A76 2′-OH group in the catalytic mechanism.

Recently, crystal structures of RF1 and RF2 in complex with 70S *T. thermophilus* ribosomes were finally determined at a medium resolution of 3−3.5 Å (*25*−*27*), thus revealing the RF−ribosome interactions in considerably more detail than earlier structures. It should, however, be noted that the P-site tRNA substrate is deacylated in these structures, thus representing a product state rather than the reactive conformation, and that the Gln side chain of the GGQ motif is apparently not methylated. Nevertheless, these first detailed structures of ribosome complexes with termination factors are a great step forward that now allows the structural basis and mechanism of the termination reaction to be explored in detail. In particular, as has been shown previously, computational analysis can play a key role in bridging the gap between structure and function by evaluating the energetics involved both in stop codon reading and in the termination reaction. Here, we report computer simulations of the peptidyl−tRNA ester hydrolysis reaction utilizing structural information from the new RF−ribosome complexes as well as higher-resolution data for binding of the substrate to the P-site. The calculations yield a consistent model for the termination reaction that reproduces experimental rates, rationalizes effects of mutations, and allows us to identify key interactions responsible for the catalytic efficiency.

MATERIALS AND METHODS

Several different systems were prepared for simulations of the peptidyl−tRNA ester hydrolysis reaction involved in translation termination. For direct comparison with earlier work (*12*), the first system was based on the high-resolution 50S *Haloarcula marismortui* structure (*22*) (PDB entry 1VQN) that contains a peptidyl-tRNA analogue (CCApcb) in the P-site and a modified puromycin aa-tRNA analogue in the A-site. The 1VQN structure was superimposed onto the 70S *T. thermophilus* complex with bound RF2 [PDB entries 2JL5 and 2JL6 (*26*)], and the A-site aa-tRNA analogue was replaced with RF2 from the 2JL5−2JL6 complex. The coordinates of C2601, A2602, and G2603 (*Escherichia coli* numbering) in the superimposed 1VQN system were replaced by the corresponding ones from the 2JL5−2JL6 structure to include the induced conformational change of A2602 upon RF binding. Otherwise, the system was prepared as described previously (*12*) with the P-site analogue CCApcb converted to CCA-Phe-Gly with the terminal amine made neutral. Crystallographic water molecules and cations were retained from the high-resolution (1VQN) structure except for a few waters causing steric clashes. The amide nitrogen of Gln240 in the conserved GGQ RF2 sequence was methylated, and a water molecule was added in a position suitable for attack of the P-site ester to give the *S*-enantiomer of the transient tetrahedral intermediate. The simulation system consisted of all residues with atoms within 20 Å of the P-site A76 O3′, where charged groups more than 15 Å from P-site A76 O3′ were neutralized as described previously to compensate for the lack of shielding at the truncated system boundary (*17*). The system was then solvated with additional water using Q (*28*) giving a total of ∼5000 atoms.

The initial structure of the second system directly used the coordinates from the 2JL5−2JL6 medium-resolution complex with bound RF2 (*26*), including the assigned cations (no water positions are available for the medium-resolution structures). The deacylated A76 in the P-site was replaced with the modeled A76-Phe-Gly substrate based on the coordinates of the CCApcb analogue from the high-resolution 1VQN structure (*22*), as described above. The C1′−N1 bond of U2585 was rotated in accordance with the 1VQN and 3D5A−3D5B structures (*25*) to prevent steric clashes between O2 of U2585 and the P-site ester. Addition of the hydrolytic water molecule, solvation, and neutralization of ionic groups close to the system boundary were performed as described above (Arg144 of the L3B protein which forms an ion pair interaction with the U2506 phosphate ester was retained in its charged form). The third system was prepared in an analogous way and directly used the coordinates from the medium-resolution 70S complex with RF1 [PDB entries 3D5A and 3D5B (*25*)], again retaining the crystallographic ions. For both of these two "medium-resolution" systems, all water molecules were thus generated by the automated solvation procedure (*28*). Two additional systems were then constructed as describe above, again based on the rRNA and protein coordinates of the 70S RF complexes (2JL5−2JL6 and 3D5A−3D5B, respectively), but now utilizing crystallographic water and ion positions from the high-resolution (1VQN) structure as was done for the first system.

The free energy surface of the ester hydrolysis reaction was calculated with the MD/FEP/EVB method (*13*, *14*). The reaction was described as previously in terms of three valence bond structures (*12*). During the simulated reaction, a proton is transferred from the attacking water to the P-site A76 O2′ and the H2′ proton is transferred to the leaving O3′ atom. Partial charges for the reacting fragments derived from ab initio HF/6-31G(d) calculations were taken from previous work (*12*). The MD simulations were performed using Q (*28*) at 300 K with the CHARMM22 force field (*29*). Atoms within the 20 Å system boundary were fully mobile, while atoms outside the boundary were restrained to their initial positions with a harmonic force constant of 100 kcal mol^{-1} $Å^{-2}$. No nonbonded interactions outside or across the boundary were calculated, and water molecules close to the boundary were restrained to reproduce the correct density and polarization (*28*, *30*). All nonbonded interactions were calculated for atoms in the reacting fragments, while for other atoms, a 10 Å cutoff was used together with a multipole expansion treatment of long-range electrostatics due to atoms outside the cutoff (*31*). The system was heated from 1 to 300 K in a stepwise manner with initial random velocities taken from a Maxwell−Boltzmann distribution. During the simulations, the temperature was kept constant by coupling to an external heat bath (*32*). The MD simulations used a time step of 1 fs, and each system was equilibrated at 300 K for ∼1 ns before data were collected.

Free energy profiles along the reaction were calculated as previously described (*12*) using the FEP/umbrella sampling approach (*13*, *14*). Each free energy calculation involved 81−101 discrete FEP steps with a 10 ps trajectory generated at each step, yielding a total of ~1 ns for each free energy profile. A large number of MD simulations were conducted with the different structural models to explore the stability of the systems and issues related to positioning of ions and water molecules. At least four independent simulations were used for final data collection for each of the five different simulation systems to evaluate the catalytic effect in ribosomes. The earlier calibration of the uncatalyzed reaction in water was also verified by multiple simulations. To allow a more direct comparison to observed hydrolysis rate constants, we now utilize the common unimolecular buffer independent values for the uncatalyzed reaction in the calibration. This gives solution free energy barriers of 26 and 25 kcal/mol flanking the transient intermediate at ~18 kcal/mol (*33*, *34*), and these values thus differ by the term *RT* ln 55 from those used previously (*12*). The exothermicity of the uncatalyzed reaction was further refined to −2 kcal/mol using this standard state and data from Jencks and Gilchrist (*35*).

RESULTS AND DISCUSSION

Overall Conformation of the GGQ Loop. One of the key issues regarding the role of the universally conserved GGQ motif in triggering the termination reaction was whether the release factor loop would insert sufficiently deeply in the A-site to make contact with P-site substrate and directly promote the attack of a water molecule on the peptidyl−tRNA ester bond. The new medium-resolution crystal structures (*25*−*27*) show that this is indeed the case as predicted by our earlier docking and MD simulations (*12*). To make this type of insertion possible, the GGQ loop must make a rather sharp U-turn that was not evident from the initial low-resolution RF complex (*6*). This type of turn is primarily enabled by the Gly residues of the loop, and Figure 1A shows a comparison of the low- and medium-resolution X-ray structures with the average loop conformation from the earlier docking/MD simulations, where all structures have been least-squares fitted to the five central Cα atoms around the Gln residue of the RF2 structure (*26*). It can immediately be seen from Figure 1A that the overall MD backbone conformation is very similar to the medium-resolution structures but that there are two peptide plane flips between the first and second Gly residue and between the Gln and following Gly residue. However, at 3−3.5 Å resolution, the electron density in this region is rather featureless (*25*, *26*) and the exact conformation of the loop might be somewhat ambiguous. Of particular interest is the orientation of the Gln backbone carbonyl group, as discussed below, and a three-dimensional motif search against the PDB using the SPASM server (*36*) shows that both of the two peptide plane conformations are, in fact, common. The root-mean-square deviation (rmsd) for the five fitted Cα atoms is 1.5 Å between the MD and RF2 structures. The corresponding difference between the RF1 and RF2 structures is only 0.3 Å as their loop conformations are virtually identical. In contrast, the GGQ loop in the low-resolution crystal structures of the RF complexes, where only a Cα trace was modeled (*6*), differs considerably from the medium-resolution structures with a corresponding rmsd of 3.0 Å. Hence, we can conclude that the docking/MD procedure was able to significantly improve the structural models obtained at ~6 Å resolution.

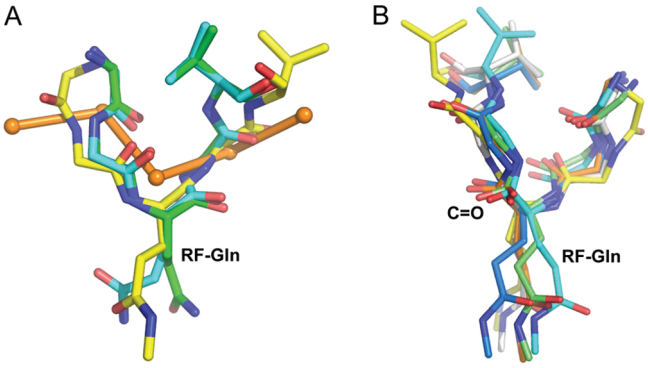

FIGURE 1: Conformation of the GGQ loop. (A) Comparison of the previously predicted GGQ loop (yellow) conformation (*12*) to that from medium-resolution structures of the RF1 (green) (*25*) and RF2 (cyan) (*26*) complexes with the ribosome. The corrsponding Cα model (orange) from the low-resolution RF−ribosome complex (*6*) is also shown. All structures are fitted to five consecutive Cα atoms centered around the Gln residue of the GGQ motif. (B) Illustration of the conformational variability of the peptide plane following the conserved Gln residue. The crystal structure of RF1 is colored dark blue together with our earlier model (*12*) (yellow) and averages from four independent simulations starting from the medium-resolution crystal structures.

Molecular dynamics simulations starting from the new medium-resolution RF structures tend to show a relatively high flexibility of the peptide plane following the conserved Gln residue, which in some simulations is observed to flip over to the conformation that it has in our earlier model (Figure 1B). This can apparently contribute to relaxing the strain of the crystallographic models and allows hydrogen bonding between the Gln carbonyl group and the 2′-OH group of A2451 (*E. coli* numbering used throughout), as an alternative to the possible hydrogen bond to the RF backbone NH group of Thr234 (RF1 numbering) indicated by the crystal structures. Here, the assignments of O versus N atoms of the RF side chain of Asn233 and rotamer of Thr234 appear somewhat ambiguous and differ between the crystal structures (*25*, *26*), and it appears that the favored orientation of the Gln peptide group may depend critically on these features. Both possible conformations of the peptide group are, however, considered below in calculations of the energetics of the hydrolysis reaction. The other peptide group that differs between our original model and the medium-resolution stuctures, between the two glycines in the GGQ motif, appears to be significantly more stable and shows no tendency to flip from the crystallographic conformation during MD simulations, although both conformations are again found to be common by SPASM (*36*).

Positioning of the Gln Residue in the PTC. A notable feature of the new RF−ribosome complex structures is the movement of A2602, corresponding roughly to a 90° rotation of its base, that allows the backbone of the GGQ loop to enter the PTC through a channel that was blocked by A2602 in earlier structures (*6*, *22*). Our earlier docking model was based on rigid ribosome structures, and such conformational changes were thus per definition not predictable. Nevertheless, apart from a relatively moderate "rotation" of the RF backbone around the Gln side chain (compared to the new structures), enforced by having a rigid ribosome, our predicted position of the Gln side chain is in very good agreement with the medium-resolution structures (*25*, *26*). Figure 2 shows a comparison between our earlier model and the RF2 complex (*26*) where the similar positioning of the

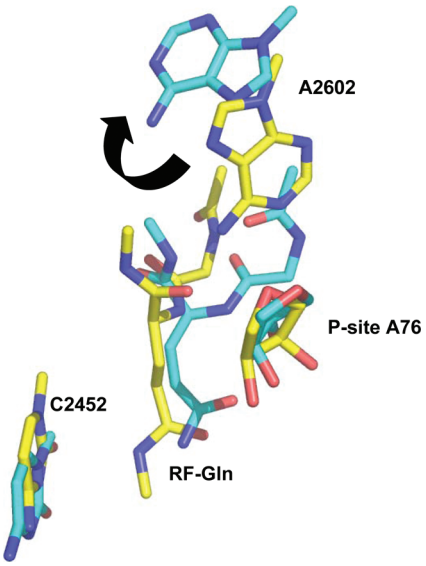

FIGURE 2: Positioning of the Gln residue in the A-site. View of the predicted positioning of the Gln side chain (yellow) from earlier docking/MD simulations (*12*) compared to the 3.5 Å resolution structure of the RF2 complex (cyan) (*26*). The movement of A2602 upon RF binding is indicated by a black arrow.

Gln side chain is clearly evident. It should again be pointed out here that the crystal structures do apparently not have the Gln side chain methylated, but it is at present unclear whether this has any significant effect on the conformation of the GGQ loop. Our simulations indicated that the main structural effect of removal of the methyl group was an increased mobility of the side chain (*12*), and recent studies of free RFs in solution do not reveal any difference in the intrinsic conformational preferences between the methylated and unmethylated GGQ loop (*37*).

As the medium-resolution RF1 and RF2 structures all have a deacylated tRNA in the ribosomal P-site, rather than the true peptidyl−tRNA substrate, one would expect some differences with respect to average MD structures of the reactive complex. Indeed, all three crystallographic complexes show a hydrogen bond between the Gln backbone NH group of the RF and the 3′-OH group of the P-site tRNA, and one of the RF2 structures also indicates a hydrogen bond between the Gln side chain carbonyl and this hydroxyl group (*26*). These hydrogen bonds are, however, not possible with a true ester substrate due to steric hindrance and the fact that the tRNA 3′-oxygen is ester-bonded. In our MD simulations, the backbone amide group instead interacts with the ester carbonyl oxygen of the substrate that also forms a hydrogen bond with an adjacent water molecule (*12*), and these interactions are preserved also in simulations utilizing the new crystal structures (see below). This interaction pattern where both the backbone NH group and a water molecule can help in stabilizing the developing negative charge on the ester oxygen also seems very logical from a catalytic perspective. It, however, appears that a slight displacement of U2585 from its position in the RF2 complex with the UGA codon (*26*) is required to accommodate a full P-site substrate, as observed in large subunit structures with substrate and product analogues (*22*).

The medium-resolution RF complex structures do not contain any information regarding water positions, and in particular, it is of considerable interest to try to identify the location of the hydrolytic water molecule in the termination reaction. Our earlier simulations placed this water molecule approximately in a "cage" formed by the Gln side chain C=O group, N3 from A2451, the 2′-OH group of A76, and the P-site ester carbon atom (Figure 3), and this model indeed predicted a large catalytic effect on the hydrolysis reaction (*12*). Upon examination of the new structures, it is striking that precisely this position of the hydrolytic water appears as the most probable, with no steric interference. It also seems to rationalize the experimental data from Green and co-workers in that a larger nucleophile would be hard to accommodate and that an interaction between the water and the 2′-OH group of A76 is possible (*23*, *24*).

Reaction Simulations Utilizing New Crystal Structures. With experimental structures of the RF−ribosome complexes, it becomes possible for the first time to explore the mechanism of the termination reaction in more detail and try to establish the origin of the catalytic effect of RFs. To this end, we carried out reaction simulations based on the experimental positions and conformation of the GGQ-containing loop, utilizing both high-resolution (*22*) and medium-resolution (*25*, *26*) ribosome structures as the starting point. The former allows for a more direct comparison of our earlier simulation model (*12*) that was based on the 1VQN *H. marismortui* 50S coordinates (*22*). A possible advantage of using the high-resolution ribosome structure in the simulations is also that it, apart from generally higher-quality atomic coordinates and the presence of a P-site substrate analogue, contains more accurate identification and positions of ions and water molecules. It should be noted that waters are completely lacking in the 3.0−3.5 Å RF−ribosome complex structures (*25*, *26*). Hence, we will first consider simulations based on combining the RF structure from 70S ribosome complexes with the 1VQN structure.

The A-site substrate analogue of the high-resolution structure (1VQN) was replaced with the RF coordinates from the RF2−ribosome complexes (*25*, *26*), and the P-site substrate analogue was converted to a hydrolyzable dipeptide attached to A76. The coordinates of C2601−G2603 were also retained from the medium-resolution complex as these bases have changed their conformation as a result of interaction with the RF. Figure 4 summarizes the free energy profiles from eight independent simulations of the termination reaction, where three of them were obtained with the 1VQN model, four were obtained with the medium-resolution structures (see below), and one curve corresponds to the results from our earlier docking model (*12*). These new simulations confirm the viability of the A76 O2′ proton shuttle mechanism, whereby transfer of a proton from the water nucleophile to the O3′ leaving group is mediated by the 2′-hydroxyl group of A76, also in the peptidyl−tRNA hydrolysis reaction. The average barrier height for the reaction of ~19 kcal/mol yields a predicted unimolecular hydrolysis rate constant of ~0.1 s^{-1}, in good agreement with experimental measurements (*23*, *24*, *38*). As one can see from these free energy curves, the two activation barriers and the stability of the transient tetrahedral intermediate are very similar in all of the different structural models. Hence, the difference in the overall positioning of the GGQ backbone with respect to our initial docking model (Figure 2) apparently has no major effect on the reaction energetics.

A key feature of all simulations is the interaction between the "oxyanion" (i.e., partially negative oxygen) of the transient tetrahedral intermediate and the backbone NH group of the methylated Gln residue, as well as the presence of a water molecule near the oxyanion that forms a stabilizing hydrogen bond to it while simultaneously interacting with the O4′ atom of U2584 (Figure 5). In this respect, the situation is similar to that in

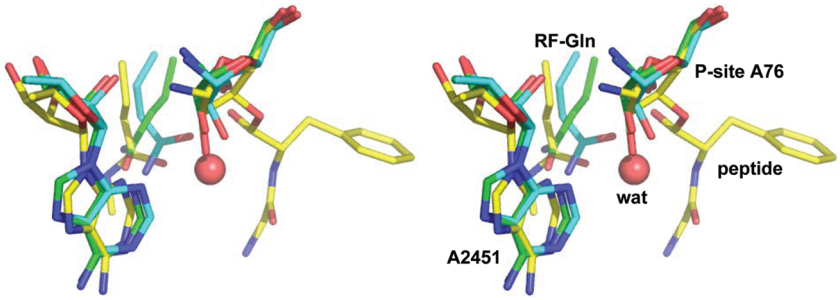

FIGURE 3: Location of the hydrolytic water molecule in the termination reaction. Stereoview of the cavity lined by A2451, the P-site peptidyl−tRNA species, and the Gln residue of the GGQ motif. The docking/MD model (*12*) is colored yellow with the water molecule depicted as a sphere. The medium-resolution RF1 (*25*) and RF2 (*26*) complexes are colored green and cyan, respectively.

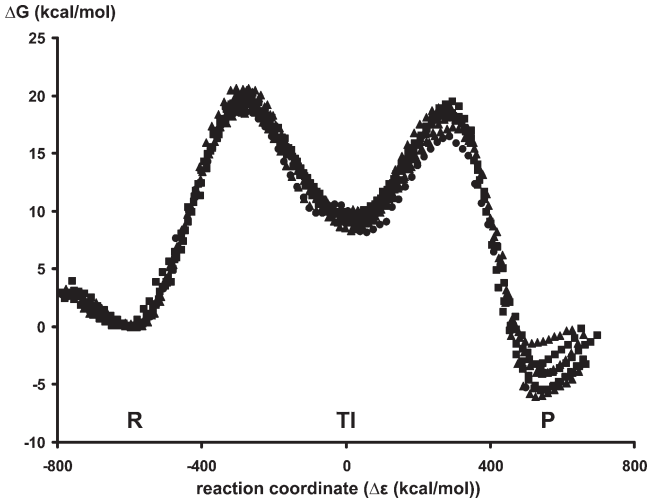

FIGURE 4: Free energy profiles for the termination reaction. Calculated free energy profiles from eight different simulations of the peptidyl−tRNA ester hydrolysis reaction. Black triangles (three simulations) denote results obtained with the high-resolution ribosome model (*22*), black squares (four simulations) results from the medium-resolution structures (*25*, *26*), and black circles the earlier results starting from our docking model (*12*). The uncertainty for the barrier heights is approximately ±1.5 kcal/mol. A generalized energy gap reaction coordinate is used (*13*, *14*), and R, TI, and P denote reactants, the tetrahedral intermediate, and products, respectively. The free energy diagram corresponds to a standard state with a water activity of unity.

peptidyl transfer, where interaction between a water molecule and the oxygen of the tetrahedral intermediate is also seen (*17*, *18*, *39*), but the backbone amide of the RF contributes an additional stabilizing element (see also ref (*25*)) that may be required because of the intrinsically slower nature of the hydrolysis reaction. As predicted previously (*12*), another essential interaction also appears to be the hydrogen bond between the Gln side chain and the attacking water molecule (Figure 5) that provides a proper orientation of the nucleophile. That this type of preorganization effect is important is apparent from the fact that reaction simulations directly employing the medium-resolution RF complex structures as initial coordinates, after methylation of the Gln residue and modeling of a proper P-site substrate, do not show any catalysis of the termination reaction (data not shown). This interesting phenomenon was traced to the positioning and assignment of crystallographic ions in these structures. Specifically, an ion assigned as Mg^{2+} near A2451 in the RF2 complex (*26*) has ligand distances of ~3 Å (rather than 2 Å), while this ion is assigned as K^+ in the high-resolution 50S structures (*22*). Further, the RF1 complex (*25*) has no fewer than five assigned Mg^{2+} ions with questionable coordination interacting with the A2450−A2453 backbone segment, which have no counterparts in the high-resolution structure where these are assigned as water molecules. These divalent ions have strong orientational effects on neighboring waters, and in both cases (RF1 and RF2 medium-resolution structures), they promote hydrogen bond networks that lead to an ~180° rotation of the methylated Gln amide group. This flip of the side chain amide dipole results in a loss of the favorable orientation of the attacking water molecule and a diminished catalytic effect.

The catalytic effect on the termination reaction was, however, recovered with the medium-resolution structures if ion and water assignments and positions were instead taken from the high-resolution structure (1VQN). In this case, coordination of the hydrolytic water molecule by the Gln side chain carbonyl is retained, and the calculated free energy profiles are shown in Figure 4. With regard to the two conformational possibilities of the backbone peptide plane following the conserved Gln, mentioned above, we find that they yield essentially identical reaction energetics, and their relevance is thus difficult to address in the absence of higher-resolution structures with transition state analogues. One can, however, note that the conformational preference of the Gln230−Gly231 peptide plane in the MD simulations appears to be coupled to the side chain conformation of Asn233 (that apparently can adopt two alternate rotamers) and that there are different hydrogen bonding alternatives involving Asn233, Thr234, and A2451 (Figure 6). The Asn is also a highly conserved residue in both RF1 and RF2 and makes hydrogen bonds to the rRNA in both of the aforementioned conformations.

To examine the origin of the catalytic effect on the termination reaction in a more quantitative way, we evaluated MD averages of the energies of interaction between the reacting parts of the substrates and nearby residues, in both the reactant and transition states. This was done for several MD trajectories that retain the crystallographic conformation of the Gln peptide plane discussed above. Figure 7 summarizes these results for groups in the immediate surroundings of the reaction center, namely, Gln230 and Asn233 of the RF, the C2063, A2451, U2506, and U2585 bases, and the three water molecules closest to the reaction center. For the RF Gln residue, the interactions are also subdivided into backbone and side chain contributions. It can be seen that in absolute terms the interactions are strongest with the Gln side chain amide dipole but that these interactions are actually stronger in the reactant state than the transition state. However, in terms of free energy, the Gln side chain contributes ~3.5 kcal/mol to the lowering of the activation barrier, corresponding to a rate factor of ~400, as deduced from thermodynamic

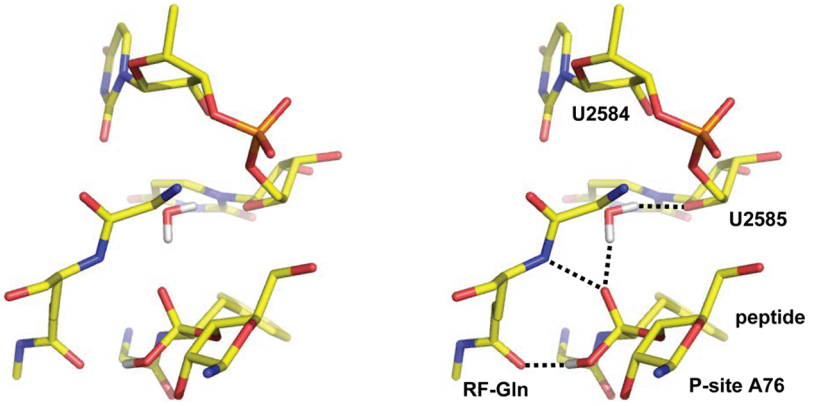

FIGURE 5: Stabilization of the transient tetrahedral intermediate. Stereoview illustrating key interactions for stabilizing the transient intermediate [representative average structure taken from a simulation utilizing the RF2 complex coordinates (*26*)]. These involve a hydrogen bond network to the partially negative oxygen of the P-site ester, provided both by the backbone NH group of the RF Gln residue and by a water molecule, as well as the interaction between the Gln side chain carbonyl group and the attacking water.

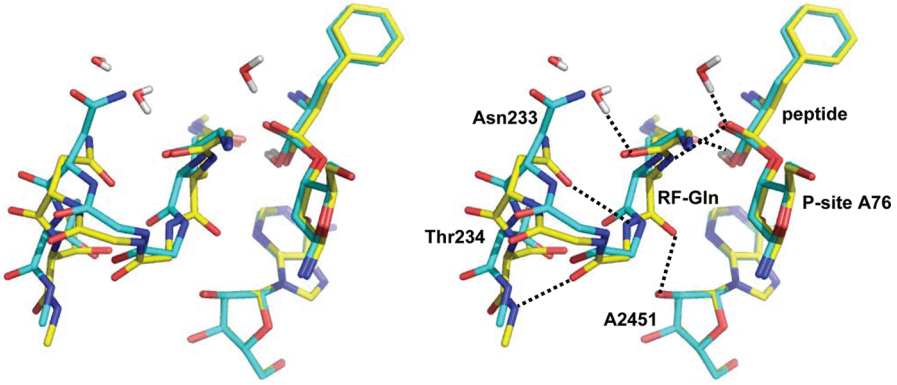

FIGURE 6: Possible conformational alternatives for the GGQ loop in catalysis. Stereoview of the average MD structures of the transient intermediate from two simulations utilizing the medium-resolution RF2 coordinates (*26*), which have different orientations of the Gln−Gly peptide plane. In the flipped conformation (yellow), relative to the crystal structures, Asn233 adopts a position where it forms a hydrogen bond to the peptide group nitrogen while its alternate polar side chain position (cyan) is replaced with water molecules (hydrogen bonds and water molecules are shown for this structure).

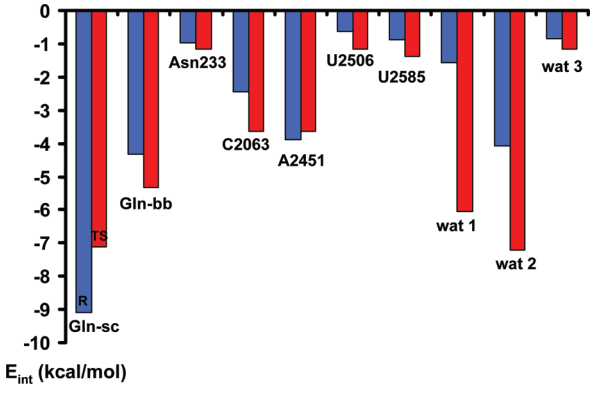

FIGURE 7: Energetics of interactions of the substrate with the PTC during the reaction. The histogram shows the average interaction energies between the reacting groups and nearby parts of the PTC, including Gln230 and Asn233 of the RF, ribosomal bases C2063, A2451, U2506, and U2585, and three water molecules. Blue and red bars denote interactions in the reactant and transition states, respectively.

integration component analysis of the free energy calculations underlying Figure 4. This analysis clearly shows that the Gln side chain amide has a favorable entropic effect on the reaction since the enthalpic contribution is positive while the free energy contribution is negative. This apparently reflects a key role of the Gln side chain in orienting the attacking water molecule. In this respect, it is therefore interesting that several Gln mutants retain hydrolysis activity (*23*) which indicates that some other side chains also could achieve a productive nucleophile coordination, perhaps with additional water molecules entering the A-site.

The Gln backbone interaction is ~1 kcal/mol stronger in the transition state, which is due to the development of negative charge on the substrate oxyanion, thus contributing an enthalpic term to its stabilization. Interactions with the nearby ribosomal bases are smaller in magnitude, and their effects on transition state stabilization are generally on the order of ≤1 kcal/mol. In contrast to the interactions mentioned above, it can be seen from Figure 7 that the water molecule hydrogen bonding to the oxyanion (wat1) provides the largest enthalpic stabilization of the transition state (~4 kcal/mol). Also, a second water molecule (wat2) in contact with both O2′ and O3′ of A76, which is observed in the high-resolution structures (*18*, *22*), contributes an enthalpic stabilization of ~3 kcal/mol. The presence of these two water molecules, which was also independently predicted in our earlier simulations of the peptidyl transfer reaction (*17*, *39*), appears to be a key feature of the reactive state of the PTC as they are observed in all relevant high-resolution complexes. That is, the hydrogen bond network identified as a major source of catalysis for both the peptidyl transfer (*17*) and termination

reaction (*12*) critically depends on a few water molecules that can bridge interactions between ribsomal groups and substrates.

Besides ribsomal release factors, it has been shown that both a deacylated cognate A-site tRNA and the CCA trinucleotide alone can stimulate hydrolysis of the P-site peptidyl−tRNA bond (*38*, *40*). Our earlier computer simulations of this process showed that O3′ of the deacylated A-site A76 can indeed precisely orient a hydrolytic water molecule that attacks the P-site ester from the *pro-S* side through the same O2′ proton shuttle mechanism as in the peptidyl transfer reaction (*12*). This prediction is also consistent with the finding that deacylated tRNA does not discriminate between water and larger nucleophiles, in contrast to the RFs (*23*). Furthermore, kinetic experiments show that the hydrolysis reaction with deacylated A-site tRNA is slowed considerably with a 2′-deoxy A76 P-site substrate (J. J. Shaw and R. Green, personal communication), supporting an A76 O2′ proton shuttle mechanism also in the termination reaction.

Crystal structures of the 50S subunit in complex with a P-site peptidyl−tRNA analogue and the di- and trinucleotides CA and CCA bound to the A-site were recently determined (*41*). These structures (PDB entries 3CMA and 3CME) confirm the prediction that the A-site A76 3′-OH group can coordinate a water molecule in a suitable position for attack on the P-site ester (*12*). The structures also show that the CA dinucleotide does not bind to the A-site in the same way as CCA or aminoacyl−tRNA analogues, as hypothesized previously (*39*). Instead, the dinucleotide is shifted outward so that CA occupies the positions corresponding to C74 and C75 in the A-site tRNA or CCA. Furthermore, these structures do not show the conformational changes of U2506 and U2585 that were the key element of the "induced-fit" mechanism proposed by Steitz and co-workers (*22*). On the contrary, the conformation of these ribosomal bases in the CA and CCA structures appears to be essentially indentical to that of the so-called uninduced structures, e.g., 1VQ6 (*22*), seemingly disproving the hypothesis that the presence of C74 is enough to induce an active conformation of the PTC.

On the basis of the CA and CCA complexes, it was further suggested that the hydrolytic water attack would occur from the *pro-R* face of the P-site ester carbon (*41*), as opposed to the *pro-S* attack of the amino group in peptidyl transfer (*17*, *22*). This proposal would seem to exclude an A76 O2′ proton shuttle mechanism in hydrolysis but offers no obvious alternative explanation for how transfer of a proton to the leaving group would occur. It also seems to be at variance with the original induced-fit hypothesis where the above-mentioned conformational changes would expose the *pro-S* face to attack from either the amino group in peptidyl transfer or a water molecule in the hydrolysis reaction. The possibility of a water attack from the *pro-R* face was said to be supported by an inferred hydrogen bond pattern in the CCA complex, which includes a hydrogen bond between N3 of A2451 (which is, however, most likely unprotonated) and the P-site ester carbonyl (*41*). Instead, we find that the most natural interpretation of the hydrogen bond pattern is rather that the free electron pairs of the attacking water are oriented away from the ester carbon in the CCA structure (1CMA), thus indicating that this might in fact not be a "reactive" structure.

CONCLUDING REMARKS

The computer simulations reported herein yield a consistent view of the mechanism of the ribosomal termination reaction, where the glutamine residue of the universally conserved GGQ motif plays a key role both in orienting the hydrolytic water molecule and in contributing to the stabilization of the high-energy intermediate and transition states of the reaction. The glutamine side chain has a significant effect on lowering of the activation barrier, and this is found to be associated with an entropic contribution. The same conclusion emerges from an analysis utilizing the linear response approximation, as in ref *42*, and shows that the entropic effect indeed has its origin in the so-called preorganization term (*43*, *44*). Besides a favorable interaction of the glutamine backbone NH group with the transition state of the hydrolysis reaction, we also find that two water molecules, observed in 50S high-resolution structures, show strong preferential hydrogen bonding to the transition state. The glycines of the GGQ motif are also clearly important in dictating the overall conformation of the loop as predicted previously (*12*, *25*, *26*). Besides reproducing observed rate constants for peptide release (*23*, *24*, *38*), the current model also rationalizes the reactivity of different nucleophiles (*23*) and the critical dependence on the 2′-OH group of the P-site substrate (*24*).

It is also notable in this context that our previous predictions for the termination reaction (*12*), regarding the overall conformation of the GGQ loop, the positioning of the Gln side chain and the hydrolytic water molecule, stabilizing interactions with the transition state, and the overall reaction energetics, are largely confirmed by simulations utilizing the new crystal structures. The main discrepancy between our previous model and the medium-resolution structures of the RF complexes is a rigid body-like movement or rotation of the RF loop backbone, leaving the position of the Gln side chain essentially unaffected, that is enabled by the movement of A2602 upon RF binding. As our earlier docking model was based on the common "rigid receptor" assumption, this conformational change was per definition not predictable. Nevertheless, one can conclude that this approach, which is often necessitated by the otherwise prohibitively large search space, can indeed be useful, although the case presented here clearly shows that induced-fit effects can also be expected in the ribosome.

The general similarity of our predicted reaction path to that proposed for the peptidyl transfer reaction (*15*−*18*), with the P-site A76 O2′ atom acting as a proton shuttle to the leaving group, is also compelling from the evolutionary viewpoint. That is, the emergence of catalytic interactions in the ribosomal PTC would clearly be facilitated by a unified type of mechanism for the hydrolysis (termination) and aminolysis (peptidyl transfer) reactions, where similar transition states occur in both processes. In this respect, it would be somewhat suprising if the peptidyl−tRNA hydrolysis reaction stimulated by binding of a deacylated A-site tRNA substrate were to proceed via a different mechanism.

ACKNOWLEDGMENT

We thank Drs. Martin Laurberg, Harry Noller, Albert Weixlbaumer, and Venki Ramakrishnan for sending us their coordinates prior to release and for providing electron density maps.

REFERENCES

1. Capecchi, M. R. (1967) Polypeptide chain termination in vitro: Isolation of a release factor. *Proc. Natl. Acad. Sci. U.S.A. 58*, 1144–1151.
2. Ito, K., Uno, M., and Nakamura, Y. (2000) A tripeptide 'anticodon' deciphers stop codons in messenger RNA. *Nature 403*, 680–684.

3. Frolova, L. Y., Tsivkovskijm, R. Y., Sivolobova, G. F., Oparina, N. Y., Serpinsky, O. I., Blinov, V. M., Tatkov, S. I., and Kissilev, L.-L. (1999) Mutations in the highly conserved GGQ motif of class 1 polypeptide release factor abolish ability of human eRF1 to trigger peptidyl-tRNA hydrolysis. *RNA 5*, 1014–1020.
4. Dincbas-Renqvist, V., Engström, Å., Mora, L., Heurgué-Hamard, V., Buckingham, R., and Ehrenberg, M. (2000) A post-translational modification in the GGQ motif of RF2 from *Escherichia coli* stimulates termination of translation. *EMBO J. 19*, 6900–6907.
5. Heurgué-Hamard, V., Champ, S., Engström, Å., Ehrenberg, M., and Buckingham, R. H. (2002) The hemK gene in *Escherichia coli* encodes the N5-glutamine methyltransferase that modifies peptide release factors. *EMBO J. 21*, 769–778.
6. Petry, S., Brodersen, D. E., Murphy, F. V., Dunham, C. M., Selmer, M., Tarry, M. J., Kelley, A. C., and Ramakrishnan, V. (2005) Crystal structures of the ribosome in complex with release factors RF1 and RF2 bound to a cognate stop codon. *Cell 123*, 1255–1266.
7. Klaholz, B. P., Pape, T., Zavialov, A. V., Myasnikov, A. G., Orlova, E. V., Vestergaard, B., Ehrenberg, M., and van Heel, M. (2003) Structure of the *Escherichia coli* ribosomal termination complex with release factor 2. *Nature 421*, 90–94.
8. Rawat, U. B. S., Zavialov, A. V., Sengupta, J., Valle, M., Grassucci, R. A., Linde, J., Vestergaard, B., Ehrenberg, M., and Frank, J. (2003) A cryoelectronmicroscopic study of ribosome-bound termination factor RF2. *Nature 421*, 87–90.
9. Vestergaard, B., Sanyal, S., Roessie, M., Mora, L., Buckingham, R. H., Kastrup, J. S., Gajhede, M., Svergun, D. I., and Ehrenberg, M. (2005) The SAXS solution structure of RF1 differs from its crystal structure and is similar to its ribosome bound cryo-EM structure. *Mol. Cell 20*, 929–938.
10. Song, H., Mugnier, P., Das, A. K., Webb, H. M., Evans, D. R., Tuite, M. F., Hemmings, B. A., and Barford, D. (2000) The crystal structure of human eukaryotic release factor eRF1-mechanism of stop codon recognition and peptidyl-tRNA hydrolysis. *Cell 100*, 311–321.
11. Verstergaard, B., Van, L. B., Andersen, G. R., Nyborg, J., Buckingham, R. H., and Kjeldgaard, M. (2001) Bacterial polypeptide release factor RF2 is structurally distinct from eucaryotic eRF1. *Mol. Cell 8*, 1375–1382.
12. Trobro, S., and Åqvist, J. (2007) A model for how ribosomal release factors induce peptidyl-tRNA cleavage in termination of protein synthesis. *Mol. Cell 27*, 758–766.
13. Warshel, A. (1991) Computer modeling of chemical reactions in enzymes and solutions , John Wiley & Sons, New York.
14. Åqvist, J., and Warshel, A. (1993) Simulation of enzyme reactions using valence bond force fields and other hybrid quantum/classical approaches. *Chem. Rev. 93*, 2523–2544.
15. Dorner, S., Panuschka, C., Schmid, W., and Barta, A. (2003) Mononucleotide derivatives as ribosomal P-site substrates reveal an important contribution of the 2′-OH to activity. *Nucleic Acids Res. 31*, 6536–6442.
16. Weinger, J. S., Parnell, K. M., Dorner, S., Green, R., and Strobel, S. A. (2004) Substrate-assisted catalysis of peptide bond formation by the ribosome. *Nat. Struct. Mol. Biol. 11*, 1101–1106.
17. Trobro, S., and Åqvist, J. (2005) Mechanism of peptide bond synthesis on the ribosome. *Proc. Natl. Acad. Sci. U.S.A. 102*, 12395–12400.
18. Schmeing, T. M., Huang, K. S., Kitchen, D. E., Strobel, S. A., and Steitz, T. A. (2005) Structural insights into the roles of water and the hydroxyl of the P site tRNA in the peptidyl transferase reaction. *Mol. Cell 20*, 437–448.
19. Seit-Nebi, A., Frolova, L., Justensen, J., and Kissilev, L. (2001) Class-1 translation termination factors: Invariant GGQ minidomain is essential for release activity and ribosomal binding but not for stop codon recognition. *Nucleic Acids Res. 29*, 3982–3987.
20. Polacek, N., Gomez, M. J., Ito, K., Xiong, L., Nakamura, Y., and Mankin, A. (2003) The critical role of the universally conserved A2602 of 23S ribosomal RNA in the release of the nascent peptide during translation termination. *Mol. Cell 11*, 103–112.
21. Amort, M., Wotzel, B., Bakowska-Zywicka, K., Erlacher, M. D., Micura, R., and Polacek, N. (2007) An intact ribose moiety at A2602 of 23S rRNA is key to trigger peptidyl-tRNA hydrolysis during translation termination. *Nucleic Acids Res. 35*, 5130–5140.
22. Schmeing, T. M., Huang, K. S., Strobel, S. A., and Steitz, T. A. (2005b) An induced-fit mechanism to promote peptide bond formation and exclude hydrolysis of peptidyl-tRNA. *Nature 438*, 520–524.
23. Shaw, J. J., and Green, R. (2007) Two distinct components of release factor function uncovered by nucleophile partitioning analysis. *Mol. Cell 28*, 458–467.
24. Brunelle, J. L., Shaw, J. J., Youngman, E. M., and Green, R. (2008) Peptide release on the ribosome depends critically on the 2′-OH of the peptidyl-tRNA substrate. *RNA 14*, 1526–1531.
25. Laurberg, M., Asahara, H., Korostelev, A., Zhu, J., Trakhanov, S., and Noller, H. F. (2008) Structural basis for translation termination on the 70S ribosome. *Nature 454*, 852–857.
26. Weixlbaumer, A., Jin, H., Neubauer, C., Voorhees, R. M., Petry, S., Kelley, A. C., and Ramakrishnan, V. (2008) Insights into translational termination from the structure of RF2 bound to the ribosome. *Science 322*, 953–956.
27. Korostelev, A., Asahara, H., Lancaster, L., Laurberg, M., Hirschi, A., Zhu, J., Trakhanov, S., Scott, W. G., and Noller, H. F. (2008) Crystal structure of a translation termination complex formed with release factor RF2. *Proc. Natl. Acad. Sci. U.S.A. 105*, 19684–19689.
28. Marelius, J., Kolmodin, K., Feierberg, I., and Åqvist, J. (1998) Q: A molecular dynamics program for free energy calculations and empirical valence bond simulations in biomolecular systems. *J. Mol. Graphics Modell. 16*, 213–225.
29. MacKerell, A. D., Wiórkiewicz-Kuczera, J., and Karplus, M. (1995) An all-atom empirical energy function for the simulation of nucleic acids. *J. Am. Chem. Soc. 117*, 11946–11975.
30. King, G., and Warshel, A. (1989) A surface constrained all-atom solvent model for effective simulations of polar solutions. *J. Chem. Phys. 91*, 3647–3661.
31. Lee, F. S., and Warshel, A. (1997) A local reaction field method for fast evaluation of long-range electrostatic interactions in molecular simulations. *J. Chem. Phys. 97*, 3100–3107.
32. Berendsen, H. J. C., Postma, J. P. M., van Gunsteren, W. F., di Nola, A., and Haak, J. R. (1984) Molecular dynamics with coupling to an external bath. *J. Chem. Phys. 81*, 3684–3690.
33. Stefanidis, D., and Jencks, W. P. (1993) General base catalysis of ester hydrolysis. *J. Am. Chem. Soc. 115*, 6045–6050.
34. Guthrie, J. P. (1973) Hydration of carboxylic acids and esters. Evaluation of the free energy change for addition of water to acetic and formic acids and their methyl esters. *J. Am. Chem. Soc. 95*, 6999–7003.
35. Jencks, W. P., and Gilchrist, M. (1964) The free energies of hydrolysis of some esters and thio esters of acetic acid. *J. Am. Chem. Soc. 86*, 4651–4654.
36. Madsen, D., and Kleywegt, G. J. (2002) Interactive motif and fold recognition in protein structures. *J. Appl. Crystallogr. 35*, 137–139.
37. Andér, M., and Åqvist, J. (2009) Does glutamine methylation affect the intrinsic conformation of the universally conserved GGQ motif in ribosomal release factors? *Biochemistry 48*, 3483–3489.
38. Zavialov, A. V., Mora, L., Buckinghan, R. H., and Ehrenberg, M. (2002) Release of peptide promoted by the GGQ motif of class 1 release factors regulates the GTPase activity of RF3. *Mol. Cell 10*, 798.
39. Trobro, S., and Åqvist, J. (2006) Analysis of predictions for the catalytic mechanism of ribosomal peptidyl transfer. *Biochemistry 45*, 7049–7056.
40. Caskey, C. T., Beaudet, A. L., Scolnick, E. M., and Rosman, M. (1971) Hydrolysis of fMet-tRNA by peptidyl transferase. *Proc. Natl. Acad. Sci. U.S.A. 68*, 3163–3167.
41. Simonovic, M., and Steitz, T. A. (2008) Peptidyl-CCA deacylation on the ribosome promoted by induced fit and the O3′-hydroxyl group of the unacylated A-site tRNA. *RNA 14*, 2372–2378.
42. Sharma, P. K., Xiang, Y., Kato, M., and Warshel, A. (2005) What are the roles of substrate-assisted catalysis and proximity effects in peptide bond formation by the ribosome? *Biochemistry 44*, 11308–11314.
43. Warshel, A., Sharma, P. K., Chu, Z. T., and Åqvist, J. (2007) Electrostatic contributions to binding of transition state analogues can be very different from the corresponding contributions to catalysis: Phenolates binding to the oxyanion hole of ketosteroid isomerase. *Biochemistry 46*, 1466–1476.
44. Almlöf, M., Åqvist, J., Smalas, A. O., and Brandsdal, B. O. (2006) Probing the effect of point mutations at protein-protein interfaces with free energy calculations. *Biophys. J. 90*, 433–442.